Diffractive optics calibrator: measurement of etching variations for binary computer-generated holograms

Wenrui Cai,* Ping Zhou, Chunyu Zhao, and James H. Burge

College of Optical Sciences, The University of Arizona, Tucson, Arizona 85721, USA

*Corresponding author: wcai@optics.arizona.edu

Received 18 December 2013; revised 5 March 2014; accepted 7 March 2014;
posted 10 March 2014 (Doc. ID 202910); published 9 April 2014

We present a new device, the diffractive optics calibrator (DOC), for measuring etching variations of computer-generated holograms (CGHs). The intensity distribution of the far-field diffraction pattern is captured and fitted to a parametric model to obtain local etching parameters such as the duty cycle, etching depth, and grating period. The sensitivity of each etching parameter is analyzed, and design choices are provided. For the wavefront created by the CGH, the DOC is capable of measuring variations in these parameters that cause 1 nm peak-to-valley phase errors. System performance is verified by measurements from a phase shift Fizeau interferometer. This device will be used primarily for quality control of the CGHs. The measurement results can be used to evaluate the fabrication performance and guide future design. DOC is also capable of generating an induced phase error map for calibration. Such calibration is essential for measuring free-form aspheric surfaces with 1 nm root-mean-square accuracy.

OCIS codes: (050.1380) Binary optics; (090.2880) Holographic interferometry; (120.4630) Optical inspection.

http://dx.doi.org/10.1364/AO.53.002477

1. Introduction

In the field of optical testing and metrology, computer-generated holograms (CGHs) are often used in interferometric systems to produce reference wavefronts. By controlling the wavefront phase of the diffracted light, the application of CGHs in optical interferometry allows complex nonspherical surfaces to be measured [1]. Fabrication errors in CGHs, however, result in errors in the diffracted wavefront, which directly affects the accuracy and validity of the interferometric measurements. Therefore, CGH fabrication errors must be either budgeted or calibrated [2].

The duty cycle and etching depth can be measured using a white light interferometer, atomic force microscope, or scanning electron microscope, which provides the surface relief of the object under test. However, these methods require expensive equipment and long inspection procedures. While they may be acceptable for small samples of diffractive optics, these methods are not suitable for inspecting large CGH substrates (usually 150–225 mm in diameter).

An alternative method is to use coherent illumination and analyze the diffraction pattern in the Fourier plane. For a diffraction grating with submicrometer features, one can use scatterometry to compare experimental data with theoretical rigorous couple-wave analysis [3–5]. In optical testing, however, the binary CGH often uses the tilt carrier to separate the desired diffraction order from other orders. The common range of the grating periods is from 5 to 30 μm, which is well within the limits of scalar diffraction theory [6]. Therefore, one can write an analytical expression for the diffraction efficiency as a function of the duty cycle and the etching depth [7,8]. This relationship is applied to a new device: the diffractive optics calibrator (DOC).

1559-128X/14/112477-10$15.00/0

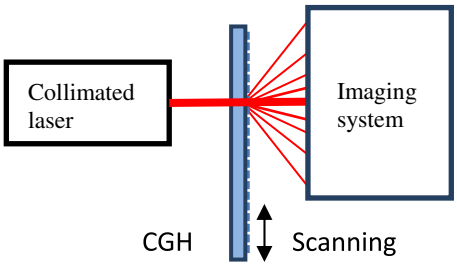

Fig. 1. System layout for the diffractive optics calibrator (DOC).

From a collimated laser beam, the intensities of multiple diffraction orders were captured by a wide-field-of-view camera lens. This measurement technique is illustrated in Fig. 1. The duty cycle and etching depth are determined simultaneously by fitting the measured intensities to a parametric model. This device is able to scan through the whole area of the diffractive optics and generate a wavefront phase error map due to variations in duty cycle and etching depth. The measurements are validated with a vertical scanning white light interferometer and a Fizeau interferometer.

The system is capable of measuring the percentage of duty cycle variation that causes 1 nm peak-to-valley (P-V) phase errors. This method is advantageous, since it can be carried out rapidly with accurate and repeatable results, does not damage the sample, and uses low-cost equipment.

In our previous works, the design, construction, and functions of the DOC were demonstrated [9]. In this paper, we focus on presenting the detailed error analysis and the operation of the DOC to measure the etching variations for a CGH. In Section 2, the Fourier mathematics for constructing the parametric model is described. The derived sensitivity functions are discussed in detail to select the proper parameters for the CGH design. In Section 3, the performance of the system is quantified by a set of calibration gratings. In Section 4, an example of using the DOC to measure the phase error induced by etching variation is presented.

2. Analysis for CGH Calibration

A. Parametric Model

The performance of a CGH is directly related to the diffraction characteristics of a linear grating. In our previous works, a binary, linear grating model was used to study the wavefront sensitivity on fabrication uniformities [2,8]. However, in microfabrication of the binary CGHs, etching may undercut the masking layer and form cavities with sloping sidewalls. In this paper, a new parameter is introduced to describe the sidewall slope in the model, which enables a more accurate prediction of the diffraction efficiency. Figure 2 depicts a cross-sectional view of a binary grating with sloping sidewalls.

The scalar diffraction approximations can be applied when the wavelength of the incident light

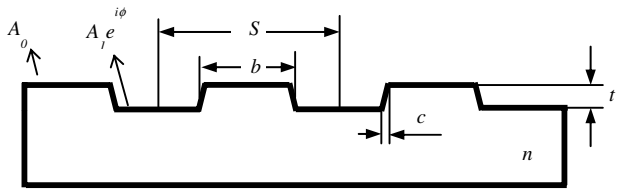

Fig. 2. Binary, linear grating profile: t is the etching depth; S is the grating period; b/S is the duty cycle; c/S is the sidewall slope ratio; and A_0 and A_1 are the amplitudes of the output wavefront from the unetched and etched areas of the grating, respectively. ϕ is the phase step between the two areas.

is much smaller in comparison to the grating period S. In this case, the output wavefront immediately past the grating, either reflected or transmitted, can be expressed as a simple product of the incident wavefront function and the grating profile function. In another words, the grating function modulates the incident wavefront directly. For a normal incident plane wavefront, the output wavefront function can be written as

$$u(x) = A_0 + (A_1 e^{i\phi} - A_0) \cdot \mathrm{rect}\left(\frac{x}{b}\right) * \frac{1}{c}\mathrm{rect}\left(\frac{x}{c}\right) * \frac{1}{S}\mathrm{comb}\left(\frac{x}{S}\right), \quad (1)$$

where the grating period is S and the etching depth is t. The duty cycle of the grating is defined as $D = b/S$, where b is the width of the unetched area. The previous square profile is replaced by the trapezoidal profile. The sidewall slope ratio is defined as $P = c/S$, where c is the width of the sidewall. A_0 and A_1 correspond to the amplitudes of the output wavefront from the unetched and etched areas of the grating, respectively. The phase depth ϕ represents the phase difference between these two areas, which equals $2\pi(n-1)t/\lambda$ for a grating used in transmission. n is the refractive index of the grating substrate.

The far-field diffraction wavefront is related to the original wavefront via a simple Fourier transform relationship based on the Fraunhofer diffraction theory. The derivations are similar to Chang *et al.*'s previous work [8]. The difference from the previous model is an additional convolution term $(1/c)\mathrm{rect}(x/c)$ in Eq. (1), which will turn into a product term after the Fourier transform.

A summary of equations for the parametric model is presented in Table 1. The wavefront phase function $\tan\Psi$ can be defined using the ratio of the imaginary part to the real part of the complex far-field wavefront function, while the diffraction efficiency η is defined as the ratio of the intensity of the diffracted wavefront to the total intensity of the incident wavefront. As functions of duty cycle and phase depth, both the zero-order and nonzero-order diffraction efficiency expressions were utilized in fitting the measured intensities. In Fig. 3, the

Table 1. Summary of Equations for Parametric Model Analysis

	Zero Order ($m = 0$)	Nonzero Order ($m = \pm 1, \pm 2, \ldots$)
	Diffracted wavefront	
η diffraction efficiency	$A_0^2(1-D)^2 + A_1^2 D^2 + 2A_0A_1D(1-D)\cos\phi$	$(A_0^2 + A_1^2 - 2A_0A_1\cos\phi)D^2\text{sinc}^2(mD)\text{sinc}^2(mP)$
$\tan\Psi$ (Ψ, wavefront phase)	$\frac{A_1 D\sin\phi}{A_0(1-D)+A_1 D\cos\phi}$	$\frac{A_1\sin\phi}{-A_0+A_1\cos\phi}$
	Sensitivity functions	
$\partial\eta/\partial D$	$-2A_0^2(1-D) + 2A_1^2 D + 2A_0A_1(1-2D)\cos\phi$	$2(A_0^2 + A_1^2 - 2A_0A_1\cos\phi)D\,\text{sinc}(2mD)\text{sinc}^2(mP)$
$\partial\eta/\partial\phi$	$-2A_0A_1(1-D)\sin\phi$	$2A_0A_1\sin\phi D^2\,\text{sinc}^2(mD)\text{sinc}^2(mP)$
$\partial\eta/\partial P$	0	$(A_0^2 + A_1^2 - 2A_0A_1\cos\phi)D^2\,\text{sinc}^2(mD)\cdot\frac{2}{P}[\text{sinc}(2mP) - \text{sinc}^2(mP)]$
$\partial\Psi/\partial D$	$\frac{A_0A_1\sin\phi}{A_1^2D^2+A_0^2(1-D)^2+2A_0A_1D(1-D)\cos\phi}$	0
$\partial\Psi/\partial\phi$	$\frac{A_1^2D^2+A_0A_1D(1-D)\cos\phi}{A_1^2D^2+A_0^2(1-D)^2+2A_0A_1D(1-D)\cos\phi}$	$\frac{A_1^2-A_0A_1\cos\phi}{A_1^2+A_0^2-2A_0A_1\cos\phi}$
$\partial\Psi/\partial P$	0	0

diffraction efficiency of order 0 to 3 is plotted versus duty cycle with 0.35λ phase depth.

Compared to the original model, the addition of a sidewall slope ratio parameter does not affect the wavefront expression; it only provides an extra term in the nonzero diffraction efficiency. In the case of anisotropic dry etching, the sidewall slopes are usually larger than 80° [10]. For example, for a binary grating with a period of 10 μm and etching depth of 500 nm, the sidewall slope ratio P is less than 1%. Since the sidewall slope ratio P is relatively small, the term $\text{sinc}^2(mP)$ gives a slowly varying envelope, which will only affect the high orders. The intensity of the seventh diffraction order will have about 1% change, which is often below the random noise level of the detector and can be ignored.

B. Sensitivity Functions

The wavefront phase sensitivity functions $\partial\Psi/\partial D$, $\partial\Psi/\partial\phi$, and $\partial\Psi/\partial P$ are defined as the deviations of the diffracted wavefront phase values due to variations in grating duty cycle, phase depth, and sidewall slope ratio, respectively. These functions are essential not only to set up the overall system requirements for DOC [11] but also to convert the measured etching variations to induced phase errors, or vice versa.

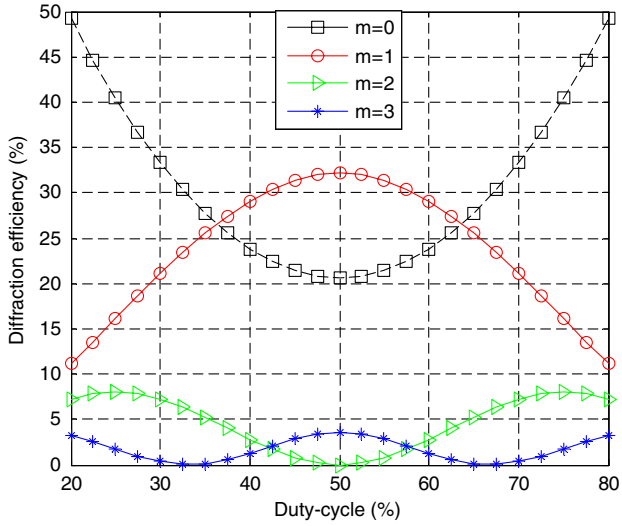

Fig. 3. Diffraction efficiency as a function of duty cycle for order 0 to 3 with 0.35λ phase depth.

As shown in Table 1, errors in the duty cycle will not introduce wavefront phase error for nonzero diffraction orders. In a special case when the duty cycle is 50% ($D = 0.5$), the wavefront phase sensitivities to etching depth are the same for all the diffraction orders.

Questions may arise here. Why bother measuring the duty cycle variations if there is no influence in the diffraction order that will be used in the optical testing (usually it is the first order)? The reason lies in the CGH substrate calibration, where the phase error of the zero order and that of the nonzero order are compared. Therefore, we are interested in the sensitivity difference between the zero and nonzero orders. The CGH substrate figure error is the dominant fabrication error, especially for a large CGH (e.g., a 150 mm by 150 mm fused silica substrate with 6 mm thickness). Since the substrate irregularity affects all the diffraction orders equally, it can be calibrated using the measurement from the zero-order diffraction. On the other hand, nonuniformities in etching parameters introduce wavefront errors for the zero and nonzero orders differently. After subtracting the zero-order measurement from the (nonzero order) surface measurement, the CGH substrate error is cancelled but the wavefront still contains some residual errors due to variations in the duty cycle or etching depth.

The variations in the duty cycle and phase depth that cause 1 nm P-V phase error between zero and nonzero diffraction orders are plotted in Figs. 4 and 5, respectively, with a range of commonly used values of duty the cycle and phase depth.

As depicted in Fig. 4, the duty cycle variation induces little phase sensitivity change as a function of the nominal duty cycle. Meanwhile, in Fig. 5, the

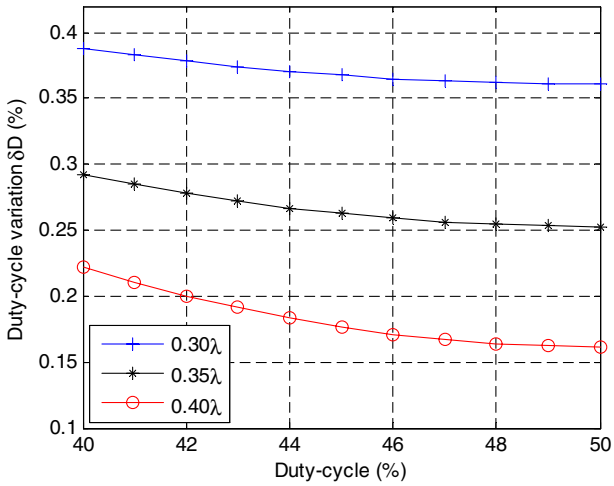

Fig. 4. Duty cycle variations that cause 1 nm P-V wavefront phase error between zero and nonzero diffraction orders.

phase depth variation induces increases in phase sensitivity as the nominal duty cycle approaches 50%. For example, there is a CGH with a 49% nominal duty cycle and 0.5 μm etching depth (0.35λ phase depth at 632.8 nm). In order to keep the error budget of the phase error induced by the duty cycle variation within 1 nm P-V, the duty cycle variation must be controlled to within 0.25% P-V, which is a demanding requirement for CGHs that have a wide range of fringe spacing.

For the same scenario, in order to keep the induced phase error within 1 nm P-V, phase depth must be controlled to within 0.03λ P-V (equivalent to about 40 nm P-V of etching depth variation), which is easily achieved for current fabrication capabilities. From this example, we can make a prediction that duty cycle variation will be the dominant contributor to the induced phase error.

The diffraction efficiency sensitivity functions $\partial\eta/\partial D$, $\partial\eta/\partial\phi$, and $\partial\eta/\partial P$ are defined as the deviations

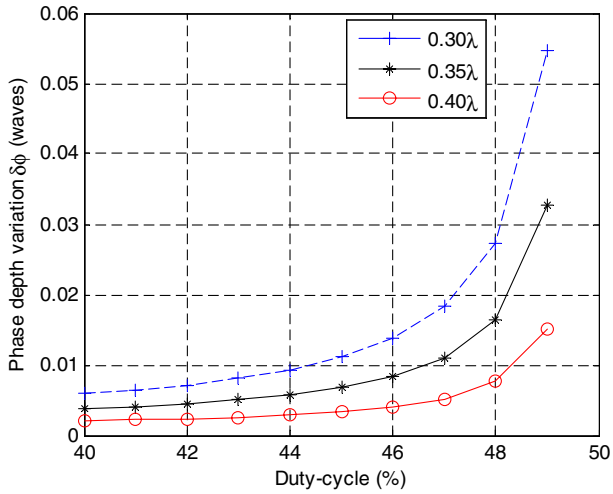

Fig. 5. Phase depth variations that cause 1 nm P-V wavefront phase error between zero and nonzero diffraction orders.

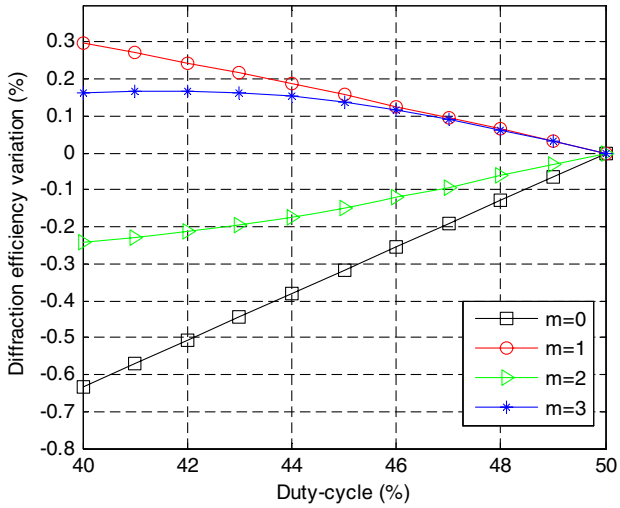

Fig. 6. Diffraction efficiency variations due to 1% duty cycle deviation. (Nominal phase depth is 0.35λ. Diffraction orders $m = 0, 1, 2, 3$ are included.)

of the diffraction efficiency due to variations in grating duty cycle, phase depth, and sidewall slope ratio, respectively. These functions are used to analyze the influence of the intensity measurement noises on the fitting results of the etching parameters.

In Fig. 6, the diffraction efficiency variations caused by 1% duty cycle deviation are plotted versus the nominal duty cycle for diffraction orders 0 to 3. The sensitivity converges to zero at 50% duty cycle. This implies that when the nominal duty cycle value is close to 50%, deviations in duty cycle have little effect on the intensity distribution among different orders. Large uncertainty occurs when using the intensity information to get a duty cycle value near 50%.

As for the diffraction efficiency variations caused by phase depth deviations plotted in Fig. 7, the

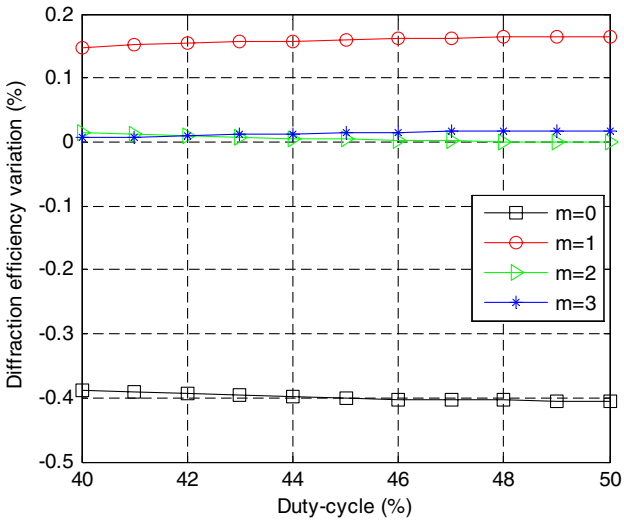

Fig. 7. Diffraction efficiency variations due to 0.01λ phase depth deviation. (Nominal phase depth is 0.35λ. Diffraction orders $m = 0, 1, 2, 3$ are included.)

sensitivity remains at the same level. In the presence of noise, with a nominal duty cycle value close to 50%, the results of phase depth (or etching depth) will be more accurate than those of duty cycle.

C. Etching Parameter Design Choice

There are reasons for choosing a duty cycle at 50% in our previous work [11]: (1) It has the maximum diffraction efficiency at the first diffraction order, which will be used in the interferometric testing. (2) The wavefront sensitivities to etching depth are the same for the zero and the first order at a 50% duty cycle, which will not generate additional residual phase error when the CGH substrate is calibrated with zero-order measurement.

However, as discussed in Section 2.B, it is difficult for the DOC to make accurate measurement near a 50% duty cycle. To illustrate this effect, a Monte Carlo simulation was performed with 0.5% random measurement noise. The fitting uncertainty shown in Fig. 8 is represented by the $1-\sigma$ standard deviation of fitting results. The uncertainties increase dramatically when the nominal duty cycle approaches 50%. Moreover, the mean value at 50% is offset by 0.3%. This is because diffraction efficiency is symmetrical about the duty cycle at 50%. As illustrated in Fig. 3, for instance, the DOC measurement cannot distinguish between 51% and 49%. Therefore, the values above 50% will degenerate into values below 50% after the fitting. In this case, the mean value will be shifted from 50%. Another consequence is that the sign of the induced phase error relative to the 50% duty cycle is unknown, while only the absolute magnitude of the induced wavefront phase error can be determined.

The characteristics of the diffraction efficiency limit the DOC's ability to perform accurate measurement when the duty cycle is about 50%. In order to utilize the DOC measurement to do calibration analysis, we proposed to choose the nominal duty cycle as 48%. The reasons are fourfold: (1) As shown in Fig. 8, at 48%, duty cycle fitting uncertainty is less than half of the uncertainty at 50%. (2) The diffraction efficiency at the first order only decreases 0.4%, compared to that at the duty cycle at 50%. (3) Assuming the etching variation of the duty cycle is less than 2%, there is no ambiguity of the duty cycle value. (4) Although phase-depth-variation-induced phase errors are different between the zero order and nonzero order, the error magnitude is negligible compared to the duty-cycle-induced phase error. It shows in Fig. 9 that the etching-depth-induced phase error at 48% duty cycle is about 8 times smaller than the duty-cycle-induced-phase error, assuming the CGH has 0.5% duty cycle variation and 5 nm etching depth variation. The black curve is the root sum square (RSS) of the two errors. The change of nominal duty-cycle has negligible impact on RSS induced phase error.

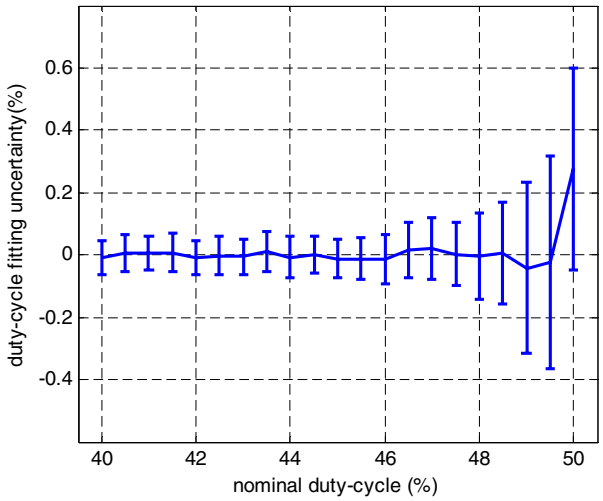

Fig. 8. Monte Carlo simulation of the duty cycle fitting uncertainty (phase depth is 0.35λ and fitting includes ± 7 orders).

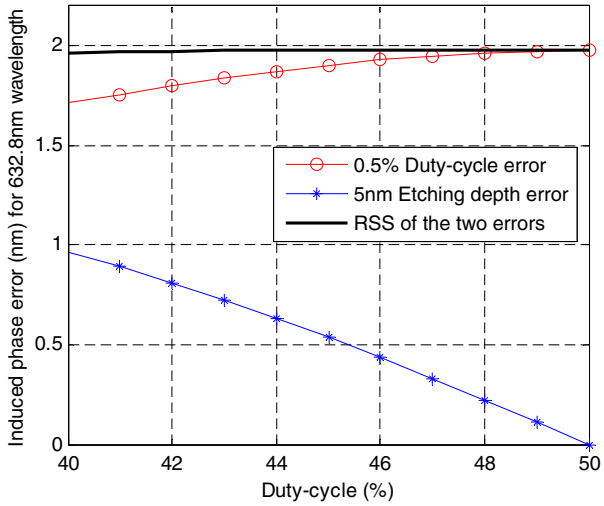

Fig. 9. Induced phase error versus nominal duty cycle value (0.5% duty cycle variation and 5 nm etching depth variation).

3. System Performance

In order to measure free-form aspheric surfaces with 1 nm root-mean-square (RMS) accuracy, the knowledge of phase error induced by etching variations must be within a fraction of 1 nm. It is shown in this section that the DOC's system performance meets this requirement.

A. DOC Hardware and Software

Figures 10(a) and 10(b) illustrate the layout of the DOC. It consists of three subsystems: optical system, mechanical system, and software. In the optical subsystem, a collimated laser beam propagates through the CGH substrate and diffracts into multiple diffraction orders. The intensities of these orders are captured by a wide-angle camera and processed via LabVIEW to obtain the local duty cycle and phase step. A two-axis motorized linear stage is implemented in the system, which is capable of scanning through a CGH with an aperture up to 225 mm In order to measure the duty cycle variation across

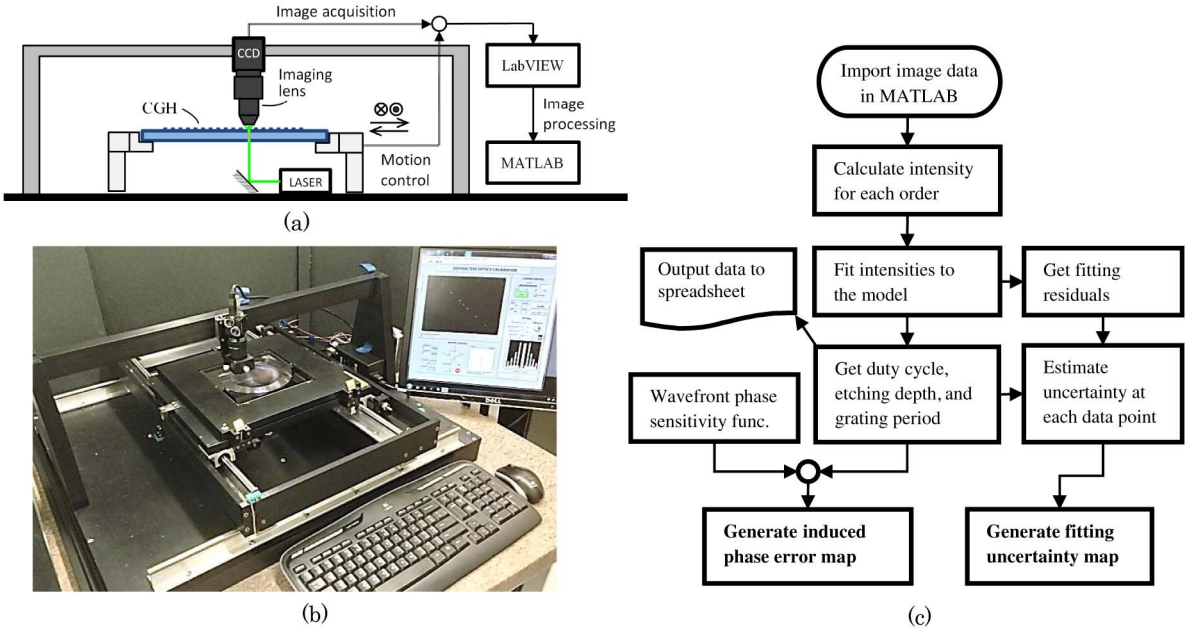

Fig. 10. (a) Schematic layout of the DOC, (b) DOC hardware with LabVIEW user interface, and (c) block diagram of the DOC measurement postprocessing in MATLAB.

the CGH aperture, LabVIEW is used to synchronize the scanning motion of the stage with the image acquisition of the camera. Detailed functions of each subsystem are discussed in our previous work [9].

To reduce the measurement time, a new procedure has been implemented for data processing with both LabVIEW and MATLAB. LabVIEW is used to do image acquisition. All the raw image data are stored with the measurement location information. Image data are then imported into MATLAB for image processing and nonlinear fitting. For example, to test a 100 mm by 100 mm CGH pattern with a 3 mm by 3 mm sampling grid, more than 1000 measurements should be taken. It takes about 1 h to finish. The procedure steps are illustrated in a flow chart in Fig. 10(c).

B. Repeatability and Accuracy of the DOC

In order to test the repeatability and accuracy of the DOC, three sets of linear gratings with varying duty cycles were fabricated. The duty cycle range is from 41% to 53%. The detail specifications of the design are listed in Table 2.

Repeatability tests were performed by measuring the same grating location multiple times. The 1σ uncertainty of the measured duty cycle values is 0.05%, and that of the measured etching depth values is 0.4 nm, which are equivalent to 0.2 and 0.01 nm RMS phase error, respectively.

Since the wavefront phase error is induced by the variation in either the duty cycle or etching depth, system repeatability is important for CGH quality control. On the other hand, the system accuracy is crucial for calibrating the induced phase error. The results between the Veeco white light interferometer and the DOC are compared in Figs. 11 and 12. The error bars are determined by the fitting uncertainty estimated by the Monte Carlo simulation result. As predicted in Section 2.C, a large discrepancy occurs at duty cycles around 50%. For the rest of the duty

Table 2. Specifications of a Set of Gratings with Different Duty Cycles

Duty Cycle Range	41% to 53% (1% change/grating)
Etching depth	0.5 μm
Grating period	15.0 μm
Grating size	3 mm × 20 mm
Overall pattern size	39 mm × 20 mm
Number of sets	3

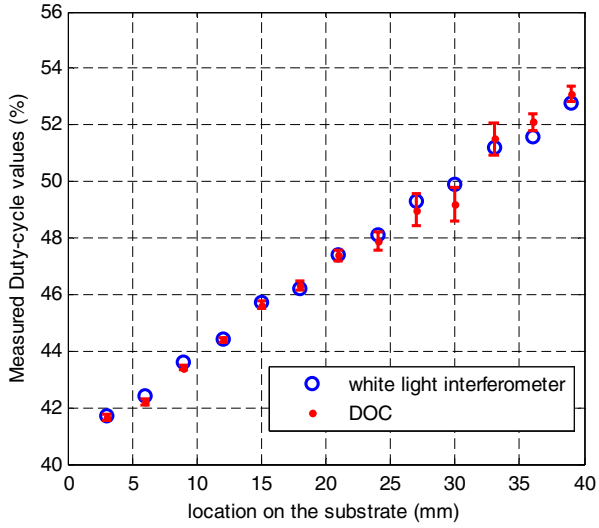

Fig. 11. Duty cycle measured values comparison between Veeco and the DOC.

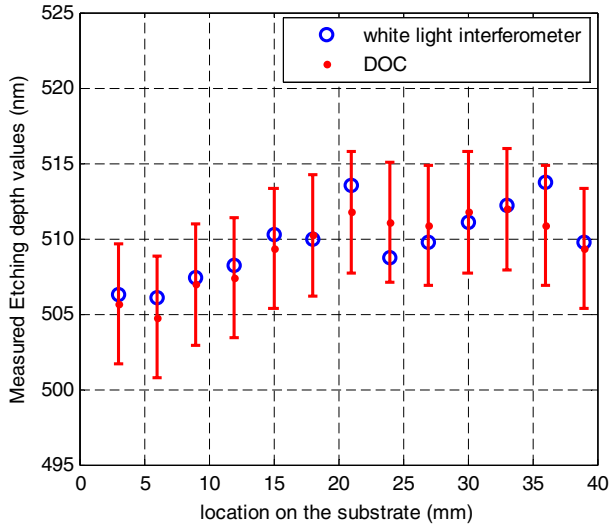

Fig. 12. Etching depth measured values comparison between Veeco and the DOC.

cycle values, the difference is around 0.25% between the two methods, which is the required accuracy to detect about 1 nm P-V phase error due to duty cycle variation. For the case of measuring etching depth, the general trends were matched for the measured values by both methods. The largest discrepancy between the two methods is 3 nm, which is equivalent to 1 nm P-V-induced phase error at a 40% duty cycle and 0.15 nm P-V-induced phase error at a 49% duty cycle.

As mentioned in Section 2.C, the DOC cannot tell if the duty cycle value is below or above 50%. We constrained the fitting results to always be less than 50%. The measured values of the duty cycle were later adjusted to be above 50% according to the nominal design.

C. Verification with Interferometric Measurement

In the previous subsection, the DOC's performance on duty cycle and etching depth measurements is verified with a white light interferometer. Once the

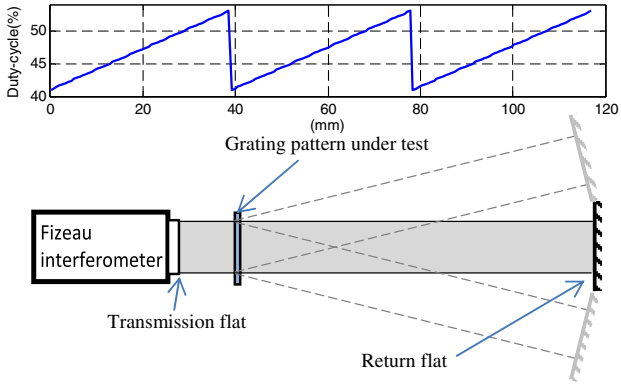

Fig. 13. Interferometric test of a pattern with three sets of gratings with duty cycle variations from 41% to 53%. The induced phase error was measured at zero order (solid line). ±1st orders were used to calibrate the grating substrate error (dotted lines).

local values on the duty cycle and etching depth are obtained, the induced wavefront phase can be calculated using the sensitivity functions in Table 1. A direct wavefront phase measurement was performed using a Fizeau-type phase shift interferometer. The same set of gratings was measured with a transmission flat and a return flat, which is depicted in Fig. 13.

CGH substrate error affects all diffraction orders equally, while the duty cycle variation only affects the zero-order wavefront. In this specific case for linear gratings, the zero order contains both the substrate error and the duty-cycle-variation-induced phase offset, while the first diffraction order contains only the substrate error. The wavefronts of the first order and the zero order were measured. The net result of subtraction of the two wavefront maps is the duty-cycle-induced phase offset, which is shown in Fig. 14(a).

The same pattern was measured in the DOC. Then the measured values of the duty cycle and etching depth were input into the wavefront sensitivity functions to generate the induced phase error map, as shown in Fig. 14(a). Although the resolution is not as good as the interferometric measurement, the induced phase error is well matched between these two methods.

The averaged profile values of the phase maps in Fig. 14(a) are plotted in Fig. 14(b). The uncertainty of the DOC measurement is the combination of the phase error from duty cycle variations and etching depth variations, which are estimated using the Monte Carlo simulation result, as depicted in Fig. 8. Other than the deviation around the 50% duty cycle mark as expected, the rest of the regions have an agreement within 5 nm with the interferometric results. This is the uncertainty level of the return flat's surface quality.

4. Application Using the DOC

In this section, we will employ the DOC to measure the etching parameters of a CGH. The information can be used in quality control and calibration. Furthermore, it also serves as feedback on the fabrication performance and future design parameter selection.

The CGH under test is a circle pattern about 90 mm in diameter. The first diffraction order generates an aspheric wavefront to be used in a null test for an off-axis parabolic mirror. As illustrated in Fig. 15(a), each fringe represents 300 fringes in the real CGH, which is equivalent to 300 waves at a 632.8 nm wavelength. The shape of the pattern stems mainly from spherical aberration and tilt. The DOC was used to measure the CGH with a resolution of 3 mm in each direction. The scanning route is depicted in Fig. 15(b).

After the scanning measurements were acquired using LabVIEW, the data were imported into MATLAB for postprocessing, including extraction of intensity information from the raw image data,

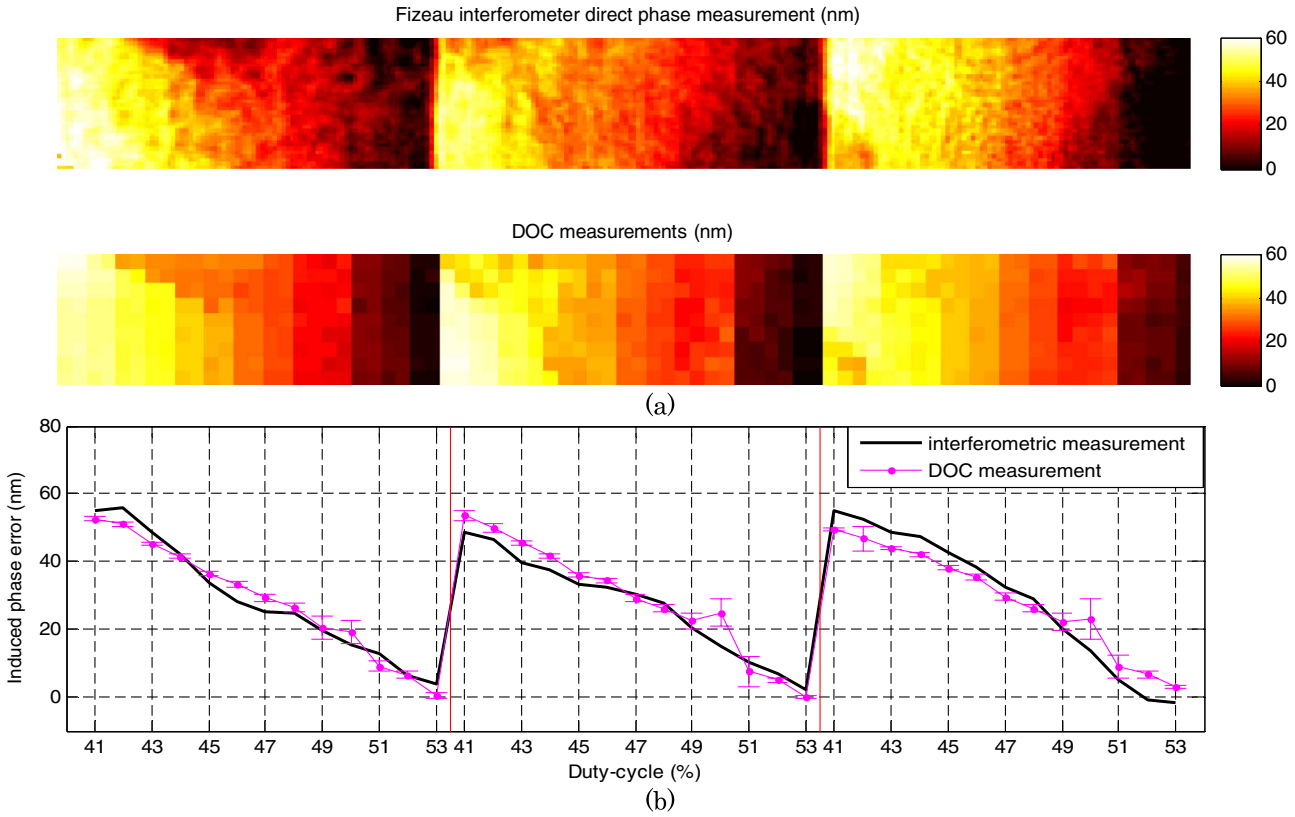

Fig. 14. Zero-order measurement comparison between interferometer and DOC. (a) Induced phase offset map comparison and (b) average phase offset profile comparison.

nonlinear least-square fitting, and generation of induced phase error maps. Detailed information of each data point, including x and y coordinates, duty cycle, etching depth, fringe spacing, and fitting residuals, was logged into a spreadsheet for future analysis.

The statistics of the measured result are listed in Table 3. Compared to the nominal design values (duty cycle is 50% and etching depth is 500 nm), the measured average duty cycle is 48%, while the measured average etching depth is 511.8 nm. This offset mainly results from the etch bias, which is the undercutting distance compared to the design of the masking layer. The amount of etch bias is usually uniform across the CGH pattern. Therefore, small features will cause more duty cycle offset by percentage.

Each parameter can also be plotted as a function of location on a 2D map, as shown in Fig. 16, which is a more intuitive way to analyze the measured result. The variations of both duty cycle and etching depth present as a shape of coma aberration in the up–down direction, which is correlated to the fringe spacing variations illustrated in Figs. 15(a) and 16(c).

Since fringe spacing is proportional to the local wavefront slope, the coma-shaped map stems from a coma-shaped wavefront slope distribution, which comes from a wavefront that contains spherical aberration. Assuming the etch bias is constant across the pattern, smaller fringe spacing will result in a larger duty cycle offset, which results in the coma-shaped variation demonstrated in Fig. 16(a). To further verify this correlation, etch bias is calculated as the product of the fringe spacing and the duty cycle offset in percentage. The etch bias map and the corresponding histogram are plotted in Figs. 17(a) and 17(b),

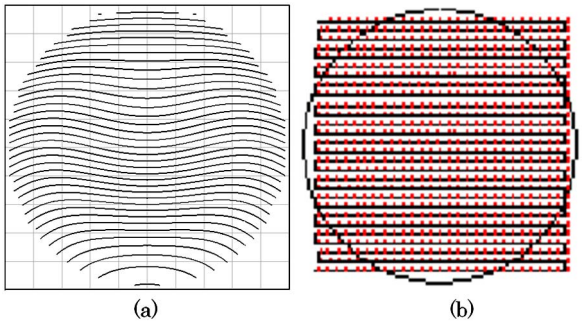

Fig. 15. (a) CGH fringe pattern representation (fringe interval = 300 waves). (b) DOC scanning route (3 mm resolution in both directions).

Table 3. DOC Measurement Results of the Etching Parameters

	Average	P-V	RMS
Duty cycle (%)	48.00	3.60	0.40
Etching depth (nm)	511.8	19.8	3.1
Fringe spacing (μm)	8.2	15.8	2.6

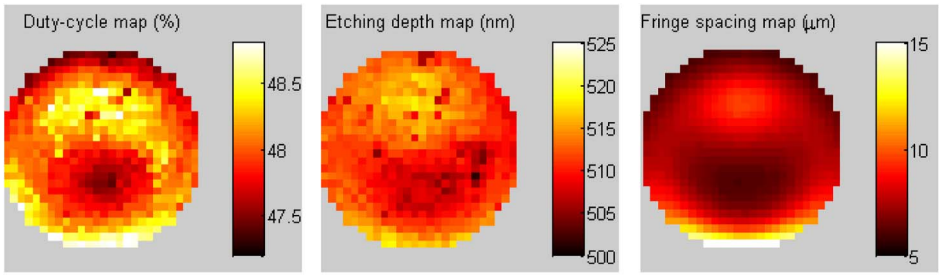

Fig. 16. 2D maps for etching parameters. (a) Duty cycle map (values in %), (b) etching depth map (values in nm), and (c) fringe spacing map (values in μm).

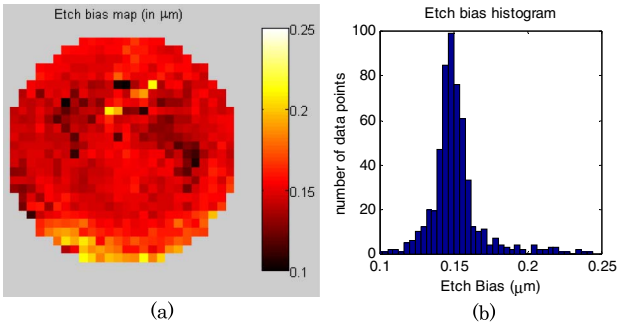

Fig. 17. The etch bias is calculated as the product of the fringe spacing and the duty cycle offset in percentage. (a) Etch bias map (values in μm), (b) etch bias histogram.

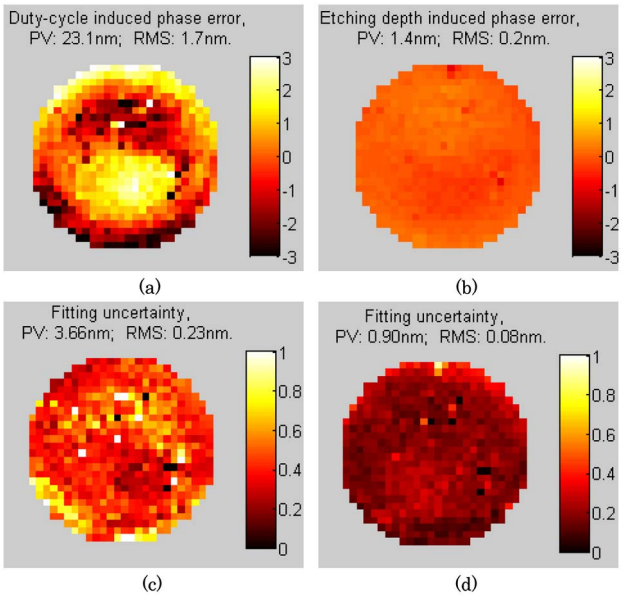

Fig. 18. Etching-variation-induced phase error maps. (a) Duty-cycle-variation-induced phase error map, (b) etching-depth-variation-induced phase error map, (c) fitting uncertainty of duty-cycle-variation-induced phase error estimated Monte Carlo simulation, and (d) fitting uncertainty of etching-depth-variation-induced phase error estimated Monte Carlo simulation.

respectively. The majority of the values are concentrated around 0.15 μm, which is an essential parameter for evaluating the etching performance. With knowledge of this fabrication error, the CGH design can be optimized to compensate the offset.

Finally, the etching-variation-induced phase error maps are generated and shown in Fig. 18. Wavefront sensitivity functions are applied to the measured duty cycle and etching depth. In Figs. 18(a) and 18(b), the induced phase errors are compared to the average value of 48% (duty cycle) and 511.8 nm (etching depth), respectively. As mentioned before, these types of induced errors are the difference between zero order and nonzero order. Therefore, when the CGH substrate error is calibrated using zero-order measurement, the phase error induced by etching variations can be taken into consideration to yield a more accurate measurement.

5. Conclusion

This paper described the DOC, a new device developed to measure the variation in duty cycle and etching depth of a binary diffractive optics used in transmission. A parametric model and the derived sensitivity functions were discussed. The system performance was quantified using a set of calibrated gratings. An example of using the DOC to measure the etch bias and the induced phase error was presented. With the exception at 50% duty cycle, the system is capable of measuring etching variations that cause 1 nm P-V phase errors in the wavefront created by the CGH. The DOC can be used to evaluate the fabrication performance and provide feedback on etching procedure and future design compensations. It can also assess the uniformity of the diffractive optics for calibration or quality control.

References

1. D. Malacara, *Optical Shop Testing*, 3rd ed., Vol. **59** of Wiley Series in Pure and Applied Optics (Wiley, 2007).
2. P. Zhou and J. H. Burge, "Fabrication error analysis and experimental demonstration for computer-generated holograms," Appl. Opt. **46**, 657–663 (2007).
3. K. Knop, "Rigorous diffraction theory for transmission phase gratings with deep rectangular grooves," J. Opt. Soc. Am. **68**, 1206–1210 (1978).
4. J. R. Marciante, N. O. Farmiga, J. I. Hirsh, M. S. Evans, and H. T. Ta, "Optical measurement of depth and duty cycle for binary diffraction gratings with subwavelength features," Appl. Opt **42**, 3234–3240 (2003).
5. V. P. Korolkov, A. S. Konchenko, V. V. Cherkashin, N. G. Mironnikov, and A. G. Poleshchuk, "Etch depth mapping of phase binary computer-generated holograms by means of

specular spectroscopic scatterometry," Opt. Eng. **52**, 091722 (2013).
6. J. W. Goodman, *Introduction to Fourier Optics*, 2nd ed. (McGraw-Hill, 1996).
7. H. P. Kleinknecht and H. Meier, "Linewidth measurement on IC masks and wafers by grating test patterns," Appl. Opt. **19**, 525–533 (1980).
8. Y. C. Chang, P. Zhou, and J. H. Burge, "Analysis of phase sensitivity for binary computer generated holograms," Appl. Opt. **45**, 4223–4234 (2006).
9. W. Cai, P. Zhou, C. Zhao, and J. H. Burge, "The diffractive optics calibrator: design and construction," Opt. Eng. **52**, 124101 (2013).
10. Z. Cao, B. Van Der Elzen, K. J. Owen, J. Yan, G. He, R. L. Peterson, D. Grimard, and K. Najafi, "DRIE of fused silica," in *Proceedings of the 26th IEEE International Conference on Micro Electro Mechanical Systems* (2013), pp. 361–364.
11. P. Zhou and J. H. Burge, "Optimal design of computer-generated holograms to minimize sensitivity to fabrication errors," Opt. Express **15**, 15410–15417 (2007).